A Newly Designed Microspectrofluorometer for Kinetic Studies on Protein Crystals in Combination with X-Ray Diffraction

Björn U. Klink, Roger S. Goody, and Axel J. Scheidig
Max-Planck-Institut für Molekulare Physiologie, Abteilung Physikalische Biochemie, D-44225 Dortmund, Germany

ABSTRACT We present a new design for a fluorescence microspectrophotometer for use in kinetic crystallography in combination with x-ray diffraction experiments. The FLUMIX device (Fluorescence spectroscopy to monitor intermediates in x-ray crystallography) is built for 0° fluorescence detection, which has several advantages in comparison to a conventional fluorometer with 90° design. Due to the reduced spatial requirements and the need for only one objective, the system is highly versatile, easy to handle, and can be used for many different applications. In combination with a conventional stereomicroscope, fluorescence measurements or reaction initiation can be performed directly in a hanging drop crystallization setup. The FLUMIX device can be combined with most x-ray sources, normally without the need of a specialized mechanical support. As a biological model system, we have used H-Ras p21 with an artificially introduced photo-labile GTP precursor (caged GTP) and a covalently attached fluorophore (IANBD amide). Using the FLUMIX system, detailed information about the state of photolyzed crystals of the modified H-Ras p21 (p21(mod)) could be obtained. Measurements in combination with a synchrotron beamline showed significant fluorescence changes in p21(mod) crystals even within a few seconds of x-ray exposure at 100 K.

INTRODUCTION

In recent years, macromolecular x-ray crystallography has progressed from being a purely static method to becoming a powerful tool for the investigation of protein kinetics at the atomic level (1–6). With the understanding that in many cases enzymatic activity can be expressed in the crystalline state, new methods have been developed for handling macromolecular crystals at room temperature (7–9), triggering reactions and accumulation of intermediates (10–14), fast data collection to monitor intermediates (15–18), and validating the state of an enzymatic reaction in macromolecular crystals (13,19–23).

One of the most problematic steps in kinetic crystallography is the validation of the state of the crystal along the reaction pathway during x-ray data collection. A commonly used technique is the destructive analysis of the crystal after data collection (e.g., by high-performance liquid chromatography (HPLC) analysis). Other methods, such as video absorption spectroscopy (13), absorption, and fluorescence spectroscopy (19,21–23) are nondestructive and therefore suitable to analyze a macromolecular crystal before an x-ray experiment. However, even if a method is nondestructive, the measurement is normally performed independent of the x-ray experiment. One major problem for the combination of nondestructive methods with an x-ray experiment is the limited space in a crystallographic setup. Many devices have to be oriented close to the crystal, limiting the space for additional equipment, such as the collimator nozzle of the x-ray source, the detector, the support for the crystal, the supply for either a humid gas stream (7,8) or a cryo-stream, an alignment camera, and additionally an optional detector for x-ray fluorescence in many experiments. For many applications, it is necessary to perform a measurement in conjunction with the x-ray experiment to obtain a direct correlation between the reaction progress and the diffraction data. As an example, Karlsson et al. (24) performed ultraviolet (UV)/visible (VIS) absorption studies in conjunction with x-ray excitation on a Rigaku RU100 x-ray generator to investigate the reduction of iron-sulfur clusters by x-ray-induced photoelectrons.

To overcome the spatial limitations of a synchrotron x-ray source, we present here a new fluorescence microspectrophotometer with 0° orientation. The FLUMIX system (FLUorescence spectroscopy to Monitor Intermediates in x-ray crystallography) has a very flexible design and can be attached to most x-ray sources. It can also be used in combination with other devices, such as a microscope, allowing reaction initiation or fluorescence measurements of macromolecular crystals directly in a hanging drop crystallization setup. The presented solution requires only one objective, which reduces spatial problems and eliminates the problem of focusing two or more objectives on the same ~50 μm spot in three-dimensional space. If a suitable light source exists, the FLUMIX system can be built up from standard components for a relatively low price, which makes it attractive as a routine tool for macromolecular crystallography.

As a biological model system, the slow GTPase H-Ras p21 was used. We introduced guanosine 5′-triphosphate P3-[1-(2-nitrophenyl)ethyl ester] (caged GTP) as a triggerable reaction educt which releases GTP and 2-nitrosoacetophenone (cage group) upon excitation with UV light in

Submitted December 1, 2005, and accepted for publication April 19, 2006.

Address reprint requests to Axel J. Scheidig, Universitätsklinikum, Geb. 60 D-66421-Homburg/Saar. Tel.: 49-6841-1626235; Fax: 49-6841-1626251; E-mail: bpasch@uniklinik-saarland.de.

Axel J. Scheidig's present address is Abteilung Strukturbiologie, Fachbereich Biophysik, Universität des Saarlandes, D-66424 Homburg/Saar, Germany.

0006-3495/06/08/981/12 $2.00

doi: 10.1529/biophysj.105.078931

the wavelength range of ~300–360 nm (25). In addition, the fluorophore *N*,*N*′-dimethyl-*N*-(iodoacetyl)-*N*′-(7-nitrobenz-2-oxa-1,3-diazol-4-yl)ethylenediamine (IANBD amide) was covalently attached to an artificially introduced cysteine (Y32C). Residue 32 is positioned in the switch I region of the protein, which is known to undergo major conformational changes upon GTP hydrolysis (26). The fluorescence properties of IANBD amide are highly sensitive to environmental changes (27), and its spectral absorption and emission bands do not overlap strongly with the excitation band of the cage group. Therefore, the fluorescence intensity can be monitored to reveal conformational changes before, during, and after the slow GTP hydrolysis reaction, which has been shown to take place even in the crystalline state of this protein (25). In addition, we have shown that after photolysis, early conformational changes during the accumulation of the GTP-bound intermediate state involve strong fluorescence changes that can be analyzed with the FLUMIX device.

In earlier work on wild-type H-Ras p21 (p21(wt)) (16,28), it was a major problem to obtain a homogenous GTP intermediate. HPLC analysis after data collection revealed that on average only one out of five crystals was sufficiently photolyzed. Furthermore, for HPLC analysis after data collection, radiolytic release of GTP from caged GTP has to be taken into account, which is especially critical for measurements using synchrotron x-ray sources (see Properties of the modified H-Ras p21 in the crystalline state). With the FLUMIX device, it is possible to obtain direct information about the state of the protein crystal, which allows a better control of the photolysis reaction and therefore an easier achievement of a homogenous GTP intermediate.

Description of the spectrometer

General design

Light sources. The layout of the spectrometer is shown in Fig. 1. An LS-1 tungsten halogen lamp (Ocean Optics, Duiven, The Netherlands) was used for alignment purposes. For fluorescence excitation, a dual-wavelength HeCd-laser (Soliton, Model IK5652R-G, Gilching, Germany) was used, which provides ~38 mW light intensity in the UV range (λ = 325 nm) and ~132 mW blue light (λ = 441.6 nm). The laser can be coupled to a 200 μm optical fiber with >75% efficiency (transmission of >100 mW blue light through the fiber, as measured with a laser power-meter (Soliton, PM-100)). Alternatively, a 150 W xenon lamp (PTI, MOD A1000) with an attached H10-UV monochromator (ISA Instruments SA, division Jobin-Yvon, Munich, Germany) can be used for fluorescence excitation. A fluorescence spectrum with 5 s integration time can be measured from a small (~50–100 μm) crystal of p21(mod)·GTP in a cryo-loop at 100 K (λ_{ex} = 441.6 nm, bandwidth 10 nm FWHM, total light intensity ~1 μW). The signal intensity reached more than 50% of detector saturation. Although the light

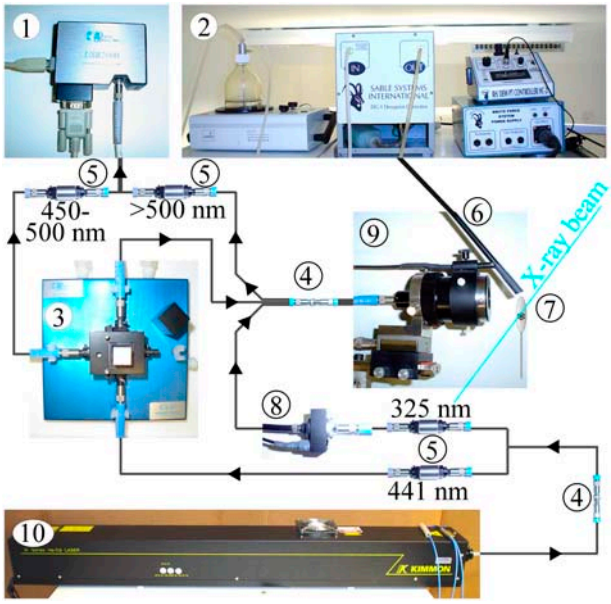

FIGURE 1 Layout of the FLUMIX spectrometer. CCD detector (*1*), humidifier (*2*), reference cuvette (*3*), fiber conjunction points (*4*), inline optical filters (*5*), humidifier nozzle (*6*), protein crystal (*7*), mechanical shutter (*8*), reflecting mirror objective (*9*), and He-Cd Laser (*10*).

from the xenon lamp might not be sufficient for kinetic studies, it is acceptable for most static applications, such as an excitation scan from a small protein crystal.

Optical fibers, inline-filters, and reference measurements. The light paths were based on optical fibers with SMA 905 connectors (Ocean Optics) and were partially designed as Y (bifurcated) or Ψ (trifurcated) fiber combinations. Inline-filters (Ocean Optics, Reference INLINE-FH) were used for the elimination of excitation light and for selection of the desired laser wavelength.

Reference measurements were performed using a cuvette holder with integrated optical fiber connections (Ocean Optics, Reference CUV-ALL-UV). For simplicity, both the reference signal and the protein fluorescence signal were detected simultaneously in a single spectrum. A narrow band-pass window (~445–485 nm, >1% transmission) of the reference signal that does not interfere with the protein fluorescence signal was selected with a long-pass (Schott, Reference GG455, Mainz, Germany) and short-pass (Schott, Reference BG4) filter combination. The reference fluorophore was 0.1 mM 7-diethylaminocoumarin-3-carboxylic acid succinimidyl ester (Invitrogen, Carlsbad, CA; Reference D1412) in dimethylsulfoxide (DMSO). Fluorescence of the reference sample is measured in conventional 90° orientation. The light that passes the reference cuvette is recoupled into the light path for fluorescence excitation of the protein crystal.

Proper design of the used fiber assemblies is crucial to reduce problems with signal instability and to maximize the detected signal intensity (Fig. 2). For example, problems with coupling efficiency can arise if two optical fibers with

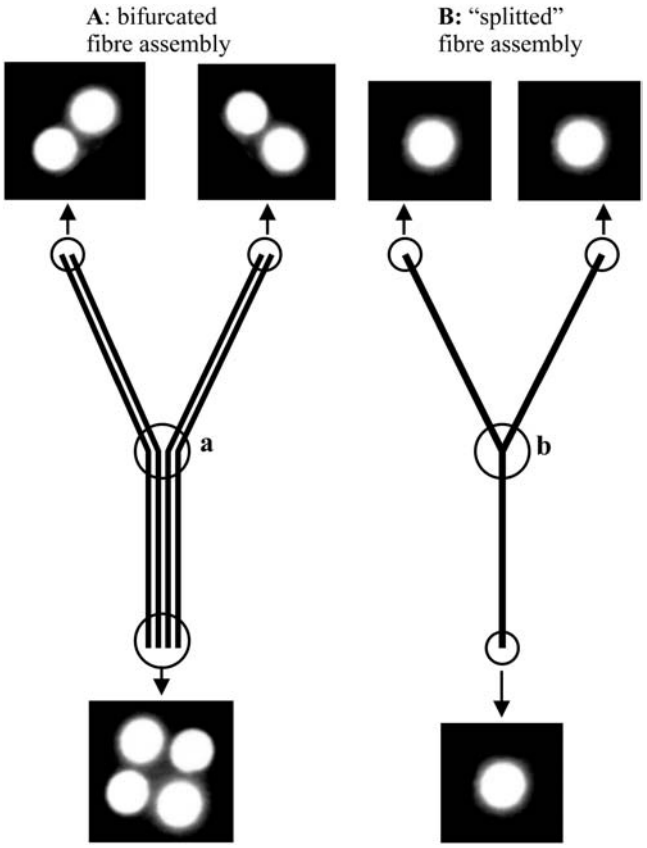

FIGURE 2 Optical fiber assemblies with different layouts. Bifurcated fibers consist of several independent fiber lines that do not interact at the conjunction point (*a*). (*A*) Typical intensity distribution at the end of a 200 μm bifurcated fiber assembly. The individual fibers are separated by a dark area with a thickness of typically ~100 μm, which cannot be avoided due to physical limitations (glue thickness, etc.). (*B*) Split fibers used to increase the coupling efficiency with connecting fiber assemblies. These fiber assemblies only use single core fiber lines, which are glued or melted together at the conjunction point (*b*). A split 200 μm fiber assembly used for the division of the laser light in one blue and one UV light path increased the effective transmission ~1.5-fold in comparison to a conventional 200 μm bifurcated fiber assembly.

very small diameter have to be connected. We found that the connection between two 50 μm fibers can involve signal fluctuations of 50% and more, most probably because the accuracy of the used fiber connectors is in the range of or higher than the total fiber diameter, resulting in poor alignment of the fibers. To avoid these problems, thin optical fibers should be avoided, or be coupled to fibers with a higher diameter. Split fibers (see Geometry of light paths and fluorescence detection) can be advantageous in this respect to replace fiber assemblies with several thin fiber lines.

Objective and objective holder. The sample was illuminated through a reflecting mirror objective with a magnification factor of 15 and a working distance of 24 mm (4DX Systems AB, Uppsala, Sweden). This objective is able to focus light into a spot size of <50 μm, producing almost no chromatic or spherical aberrations (21).

Only one objective is needed for the presented setup (see Geometry of light paths and fluorescence detection), which made the design of a suitable objective holder relatively unproblematic. The holder consists of a strong NeFeB magnet base plate with ~100 kg lifting capacity, a triangular metal block that is glued to the magnet, and three identical metal bars that can be screwed to the block to form an adjustable arm (Fig. 3). The reflecting mirror objective can be mounted to the final metal bar. The objective is equipped with integrated X-Y-Z fine adjustments, so that only the prealignment has to be done by proper orientation of the components of the objective holder. Due to the available degrees of freedom, almost every desired orientation of the objective can be achieved, which simplifies the combination with other devices (see Different spectrometer layouts).

Geometry of light paths and fluorescence detection. The FLUMIX device is designed for 0° orientation, which means that fluorescence excitation and signal detection is performed through the same objective. This has several advantages in comparison to a 90° design: First, the reduced spatial requirements due to the need of only one objective make it much easier to combine the fluorescence detector with an x-ray source or other devices, and the objective holder is relatively

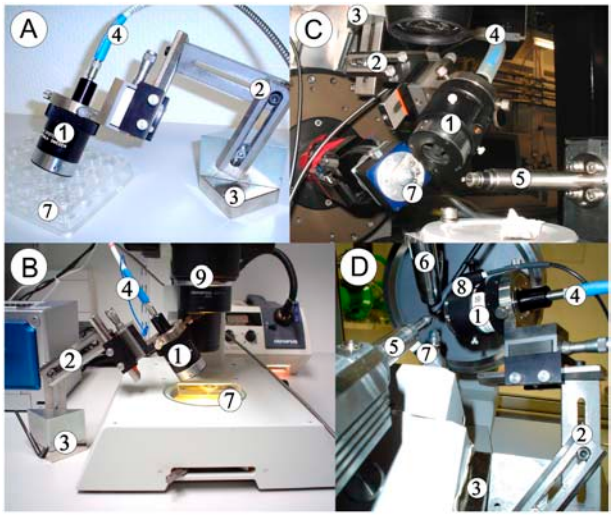

FIGURE 3 Different applications for the FLUMIX device. (*A*) The FLUMIX device attached to a hanging drop crystal setup, (*B*) to a stereomicroscope (9), (*C*) to a synchrotron beamline (SLS, PSI Villigen, PX-I), and (*D*) to an x-ray home source (Oxford Diffraction, Xcalibur PX Ultra). The objective (*1*) of the FLUMIX device is attached via a flexible arm (*2*) and a NeFeB-magnet base plate with ~100 kg lifting capacity (*3*). The magnet can be attached either directly to a magnetic metal support, or via a second magnetic plate positioned below a nonmagnetic plate to keep the objective holder in place (e.g., when using the holder on a lab bench, as shown in *A* and *B*). An optical fiber assembly (*4*), which is connected to the reflecting mirror objective (*1*), divides the light into the different light paths for excitation and fluorescence detection. An x-ray beam emerging from *5* is not disturbed by the setup, allowing fluorescence measurements in combination with x-ray diffraction experiments. The protein crystal (*7*) can be kept stable by a nitrogen stream at cryogenic temperatures (*6*) or by a humid gas stream (*8*) at ambient temperature.

easy to design. Second, the alignment to the crystal is much simpler than the alignment of two objectives to the same point in three-dimensional space. Finally, a measurement in front-face geometry (29) has the advantage that even samples with very high optical density can be analyzed. For interpretation of the results; however, one should take into account that the fluorescence measurement does not necessarily represent the state of all molecules within the crystal volume (21). This can be critical in a photolysis experiment if only the surface of the crystal is photolyzed, but in a concomitant x-ray diffraction experiment a data set is measured from the whole volume of the macromolecular crystal. For the laser wavelengths of the HeCd-laser; however, the optical density of the used crystals is low enough to allow an almost homogenous excitation for crystals with a size of $\sim$50 μm (see Development of the biological model system; H-ras p21).

To connect the different spectrometer components (UV excitation light path, blue excitation light path, and fluorescence detection light path) with the objective, a trifurcated fiber with seven individual fiber lines was used, each with a thickness of 100 μm. Four of the seven fiber lines are used for signal detection, two fibers for UV (325 nm) photolysis and only the center fiber (which generates the lowest amount of intensity fluctuations) for fluorescence excitation (441 nm).

In a fiber bundle with several individual fiber lines, each fiber line has its own focal spot position, which can lead to problems if the overlap between the focal spots of the exciting and the detecting fibers is too low. The spot size of the reflecting mirror objective used is $<$50 μm, and the minimum distance between the individual fibers in a fiber bundle is normally $\sim$100 μm (Fig. 2). This means that with direct connection of a trifurcated fiber assembly to the objective, the focal spots of the fiber lines for excitation and detection would be spatially separated, resulting in a low fluorescence signal. To avoid this problem, the trifurcated fiber assembly was coupled to an additional single core fiber with a large diameter (400 μm), and this fiber was attached to the objective. This ensures that the focal spots for detection and excitation are exactly identical (assuming that all light is evenly distributed within the 400 μm optical fiber). By adding the additional fiber, similar fluorescence signal intensities could be achieved with significantly lower photon density and therefore less thermal stress on the protein crystal. Additionally, a more homogenous excitation of the crystal is achieved due to the higher resulting focal spot diameter when using the 400 μm fiber, which is especially advantageous for the release of caged compounds or other reaction initiation methods that are based on excitation by light.

Sample manipulation at room temperature. For unfrozen samples, a DG-1 humidity controller (humidifier) (Sable Systems, Las Vegas, NV) was used to deliver a stream of air or nitrogen with adjustable humidity. A simple humidifier nozzle was designed, which can be directly attached to the reflecting mirror objective to minimize the required space around the crystal for this additional component. In this nozzle, a temperature sensor can be located close to the exit of the gas stream. This sensor is necessary for continuous feedback with the humidifier to generate a stable relative humidity even with fluctuating room temperature. To allow relative humidity values of close to 100%, a type 8901 wax warmer (Babor Treatment Systems) was used to heat the water reservoir bottle of the humidifier a few degrees above ambient temperature. As described by Kiefersauer et al. (8), a humidifier can be used for keeping protein crystals stable in a standard cryo-loop at room temperature for many hours. By precise manipulation of the humidity (shrinking), an increase of the diffraction quality of macromolecular crystals is possible in many cases.

CCD detector and analysis software. The fluorescence signal was detected using a USB 2000 monolithic fiber optic spectrometer (Ocean Optics). It consists of a 200 μm entrance slit, a 600 lines/mm grating (Ocean Optics, grating No. 2) and a 2048-element linear silicon charge-coupled device (CCD) array. The maximum signal/noise ratio is $\sim$250:1, and the spectral resolution $\sim$7.5 nm.

Analysis was performed with the software package OOIBase32 Platinum (Ocean Optics, Program Version 2.0.1.4). The embedded Visual Basic scripting language allows specific data collection protocols and sophisticated control of external devices, such as the external mechanical shutter (Ocean Optics, Referernce INLINE-TTL-S) that can be directly attached and synchronized with the CCD detector. With this option, applications such as the detection of a fluorescence spectrum every few minutes with a closed light path during the rest of the time can be implemented, which helps to minimize fluorescence bleaching in long time-based experiments.

Different spectrometer layouts

Layout for fluorescence detection and reaction initiation in hanging drop crystals

The most common technique to grow protein crystals uses a hanging drop setup, where a droplet of a mixture containing the macromolecular substance of interest and a precipitant solution hangs from a cover slide above a precipitant solution. The concentration of the macromolecular solution increases slowly due to vapor diffusion between the droplet and the precipitant solution. If the crystallization conditions are appropriate, crystal formation begins after the concentration reaches a critical level (30).

Under certain circumstances, it is possible that the protein crystal of interest changes its properties during crystal growth. In the example presented here, although caged GTP is resistant to hydrolysis by H-Ras p21, there is a slow light independent decay to GDP and caged P_i in the crystal (31). For the p21(mod) used in this work, HPLC analysis revealed that S-caged GTP showed a significantly higher rate of decay

to caged P_i and GDP (80% hydrolysis within 100 days) than R-caged GTP crystals (22% hydrolysis within 100 days), as was also observed for the wild-type protein (31). Since the fluorescence properties of p21(mod) crystals change upon caged GTP hydrolysis, it is possible to analyze this intrinsic GTPase activity with the FLUMIX device. Another example is NAD(P)-binding proteins where the oxidation state of the nucleotide might change during the crystallization process. Since only the reduced form NAD(P)H is fluorescent, the oxidation state can be easily monitored using the FLUMIX device.

The advantage of the presented 0° fluorescence detection strategy is that growing protein crystals can be analyzed without removing the crystals from the hanging drop setup. Absorption measurements with a 180° orientation of the optical components cannot easily be performed for such setups with the commonly used crystallization plates due to their optical properties. In principle, fluorescence spectroscopy at 90° orientation could be performed, but due to the high and unpredictable distortion of the light path by the cover slide and the crystallization droplet, proper alignment of two objectives would be very complicated.

With the presented setup, such an experiment is straightforward since the light paths for excitation and detection are identical. A rough alignment of the objective can be achieved by positioning the objective holder so that the objective illuminates the protein crystal, which can be observed with a conventional stereomicroscope. The focus of the objective can be fine-adjusted by maximizing the detected fluorescence intensity. The homogeneity of excitation of the crystal can be verified by visual inspection of the excited crystal area with the stereomicroscope. For light intensities that are too high for direct observation, a video adaptor can be connected to the microscope (Fig. 3 *B*).

Layout for the FLUMIX device attached to a conventional (home-source) x-ray diffraction setup

For fluorescence measurements in conjunction with x-ray diffraction, the objective holder has to be attached to the x-ray source without interference with the rest of the setup. With the used orientation on an Xcalibur PX Ultra x-ray generator (Oxford Diffraction, Abington, England) (Fig. 3 *D*), it is possible to measure a complete data set from crystals with sufficiently high symmetry without changing the orientation of the crystal with respect to the fluorescence detector. This is very helpful if fluorescence changes during an x-ray diffraction experiment need to be measured. For such an experiment, the scan is performed using the omega-axis of the kappa-diffractometer. It is possible to scan ~90° before the fluorescence detector collides with the x-ray detector.

Measurements can be performed on frozen samples using the cryo-jet of the Xcalibur system. For unfrozen samples, a humid gas stream generated by a DG-1 humidity controller (humidifier) (Sable Systems, Int.) was used to stabilize the sample in a nylon-loop at ambient temperatures (see Sample manipulation at room temperature).

Layout for the FLUMIX device attached to a synchrotron beamline

We have attached the objective to three different synchrotron setups (ID14-3 and ID14-2 at ESRF, Grenoble; and PX-I at SLS, PSI Villigen). In all cases, the objective holder could be attached and the objective could be oriented to the protein crystal without the need of a specialized mechanical support. One layout that was used at the PX-I beamline for fluorescence measurements in correlation with x-ray diffraction is shown in Fig. 3 *C*. With small modifications to the setup, either a humid gas stream or a cryo-stream could be used to stabilize the samples at ambient or cryogenic temperatures, respectively.

Development of the biological model system H-ras p21

As a biological model system, we decided to use a protein that has no intrinsic reaction trigger and no fluorescence in the visible range. The protein was modified such that kinetic fluorescence studies could be performed to show the general applicability of this method for macromolecular crystals.

H-Ras p21 is a small guanosine nucleotide binding protein with low GTPase activity that is involved in signal transduction pathways. Upon GTP hydrolysis, which takes place on the several minutes timescale, the protein changes from an active GTP-bound state to an inactive GDP-bound state. It was shown that the involved conformational changes can even take place in the crystalline state, without destroying the crystal order (25).

For the introduction of a fluorescence probe, a truncated form (aa 1–166) of the protein with two additional mutations (Y32C and C118S) was used. Residue 32 is located in the switch I region of the protein, which is one of the regions that undergo major conformational changes upon GTP hydrolysis. Cys-118 was replaced by serine to prevent double labeling of the protein. The remaining two cysteines, Cys-51 and Cys-80, are not surface exposed and could not be labeled under the reaction conditions used.

GDP that is bound to the protein at a stoichiometric ratio after purification was exchanged against the isomerically pure forms of caged GTP, according to a method developed by Scherer et al. (32). R/S-caged GTP serves as a nonhydrolysable reaction educt that can release GTP upon excitation with UV light of 300–360 nm. The C32 position was labeled with the thiol-reactive fluorophore IANBD amide. Stoichiometric labeling of the Y32C position was verified by NTCB digestion and mass spectroscopy (B. U. Klink and A. J. Scheidign, unpublished). The fluorescence yield of the 7-nitrobenz-2-oxa-1,3-diazole-4-yl (NBD) fluorophore is known to be highly sensitive to environmental changes (27) and could therefore be used for monitoring conformational changes within the protein. Additionally, it has a fluorescence excitation

maximum that does not overlap with the maximum of photolysis efficiency of caged GTP. Furthermore, the large Stokes shift of this fluorophore allows an efficient separation of the fluorescence excitation light from the emission spectrum. Crystals with high diffraction power (up to ~1.05 Å resolution) of the modified protein H-Ras p21 (aa 1–166, Y32C, C118S, C32-IANBD-amide)·Mg^{2+}·R/S-caged GTP) (p21(mod)·R/S-caged GTP) could be grown, and by proper modification of the crystallization conditions, different crystal forms and sizes could be obtained reproducibly. For photolysis experiments, crystals with a thickness of ~50 μm were used to guarantee a sufficiently low optical density of the crystals. We extrapolated the optical density of such a 50 μm crystal to be ~0.59 at 325 nm and 0.94 at 441 nm.

RESULTS

Specifications of the FLUMIX device

As a reference substance to compare different layouts of the spectrometer, we analyzed a 0.4–0.5 mm cryo-loop filled with 0.3 mM disodium fluorescein in 40% glycerol at 170 K. These sample conditions are similar to those used by Bourgeois et al. (21). Since different laser wavelengths and other parameters such as sample size and orientation can significantly affect the measured signal intensity, the comparison can only be qualitative. Due to solubility problems with pure fluorescein, we used the disodium salt. We observed that the absorption maximum of disodium fluorescein in 40% glycerol at ambient temperature shows a single absorption peak at ~493 nm for concentrations >1 mM, and between 1 and 0.3 mM the maximum shifts to a double peak at ~450 and 477 nm. The absorption maximum of ~490 nm for a 0.3 mM solution of fluorescein reported in (21) might be due to the different temperature at which the spectrum was collected, due to the use of fluorescein instead of the disodium salt, or due to a slight concentration increase of the solution during the mounting procedure in a cryo-loop.

The fluorescence spectra measured with different setups are shown in Fig. 4 *A*. As can be seen, with the setup used for most experiments similar signal intensities as reported by Bourgeois et al. (21) were obtained, using only ~1 mW blue light intensity for fluorescence excitation (Fig. 4 *A*, spectra *3* and *4*, respectively). With small modifications in our setup, the measured signal intensity can be increased further by a factor of more than 15 (Fig. 4 *A*, spectrum *1*), causing detector saturation within <7 ms integration time. For the latter, both excitation pathways were used, increasing the total excitation intensity to ~2 mW. Only the detection light path was connected to the detector to maximize detection efficiency. The reference light path was not connected, although the reference cell was kept in line. This would be the optimal configuration if a second detector channel for the reference were available and if only single wavelength excitation were needed.

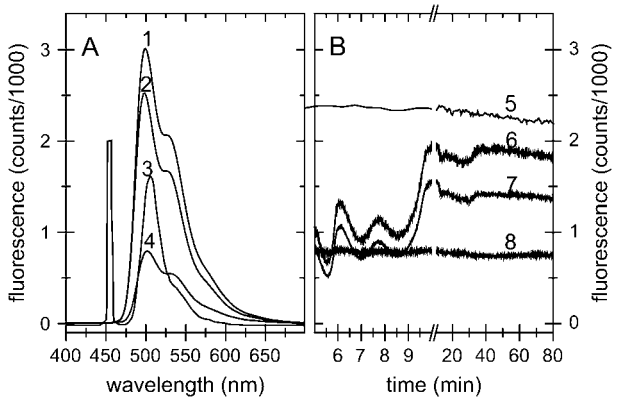

FIGURE 4 Signal intensity and stability measurements. (*A*) Fluorescence spectra (λ_{Ex} = 441.6 nm) of disodium fluorescein (0.3 mM in 40% glycerol at 170 K) fixed as a drop in a 0.4–0.5 mm cryo-loop. For spectra taken with a layout as described in Fig. 1, the integration time was 20 ms (trace *4*). An integration time of 5 ms was used for spectra taken with the setup using both excitation light paths for fluorescence excitation and omitting the light path from the reference cuvette to the detector (trace *1*) and for the same setup with the trifurcated fiber assembly directly attached to the objective (trace *2*). For comparison, a spectrum measured by Bourgeois et al. (21) with 20 ms integration time (trace *3*) is shown. (*B*) Stability measurements on disodium fluorescein (λ_{Em} = 513 nm) (trace *5*) displayed an rms deviation of 0.68% and a linear signal decrease of 6.0% per h. For this measurement, the laser light source was allowed to stabilize for several hours. During the first ~15 min after ignition of the He-Cd laser, strong intensity fluctuations occur, which can be corrected for by a reference measurement as described in Optical fibers, inline-filters, and reference measurements. Reference signal (λ_{Em} = 470 nm) using 0.1 mM 7-diethylaminocoumarin-3-carboxylic acid, succinimidyl ester (Invitrogen, Reference D1412) in DMSO, multiplied by a factor of 10 (trace *6*). Uncorrected spectrum from a sample of p21(mod)·GDP in a cryo-loop at 100 K (λ_{Em} = 540 nm) (trace *7*). Corrected spectrum of p21(mod)·GDP: (spectrum *7*)/(spectrum *6*)·2000 (trace *8*). The corrected spectrum (trace *8*) displays an rms deviation of 1.0% in the first 5 min, where the strongest intensity fluctuations occur, and ~0.75% after stabilization of the laser.

It is of interest to note that the additional 400 μm single core optical fiber between the objective and the connected trifurcated fiber assembly results in slightly increased signal intensity, despite the fact that the light intensity that enters the objective is decreased from ~3 mW to ~2 mW due to the additional fiber conjunction point. We conclude that the advantage of an identical focal spot for the excitation and detection light paths overcompensates the intensity loss due to the additional fiber connection. The lower photon density on the sample and a more homogenous excitation due to the increased spot size additionally favor this layout for most experiments on protein single crystals.

An uncorrected and a corrected measurement on p21(mod)·GDP are shown in Fig. 4 *B*. As can be seen, fluctuations in the intensity of the light source can be adequately corrected for with the chosen reference measurement strategy. The corrected spectrum (Fig. 4, spectrum *8*) displays a root mean-squared (rms) deviation of 1.0% in the first 5 min, where the strongest intensity fluctuations occur, and ~0.75% after stabilization of the laser.

In addition, the signal stability of an uncorrected measurement of disodium fluorescein (sample conditions as above) in a cryo-loop is shown (Fig. 4 *B*, spectrum *5*). Before this measurement, the laser was allowed to stabilize for several hours. A linear fit of this spectrum displayed an rms deviation of 0.68% and a linear signal decrease of 6.0% per h in the uncorrected sample.

Properties of modified H-Ras p21 in solution

The GTPase activity of p21(mod) was investigated using HPLC and fluorescence measurements. The fluorescence experiments were performed in a hanging drop setup, as described in Layout for fluorescence detection and reaction initiation in hanging drop crystals ($T = 21°C$, pH 7.6). The photolysis of caged GTP in p21(mod)·R-caged GTP results in a fluorescence decrease by a factor of 1.8. Upon GTP hydrolysis, the fluorescence intensity further decreases by ~20%. The latter fluorescence decay can be adequately fit with a single exponential decay with a half-time of $t_{½} = 384 \pm 7$ min. This is in good agreement with HPLC analysis, where a half-time of $t_{½} = 430 \pm 18$ min for the GTP hydrolysis reaction was calculated. According to these results, the modified form of H-Ras p21 has a significantly reduced GTPase activity in comparison with the truncated wild-type form of H-Ras p21 ($t_{½} = 18.7$ min at 37°C (33)).

The significantly reduced GTPase activity of the modified protein must result from the introduced fluorescence label attached to residue 32 in the switch I region. It is well known that the switch I region can adopt different conformations. Therefore, it is likely that in the modified protein, conformations are favored that are not optimal for GTP hydrolysis. However, this does not limit its use for the performed measurements. In fact, the reduced GTPase activity can simplify the accumulation of the homogeneous metastable GTP-bound state of the protein.

Properties of the modified H-Ras p21 in the crystalline state

The GTP hydrolysis halftime in p21(mod) crystals at room temperature was estimated by HPLC measurements on photolyzed p21(mod)·R-caged GTP crystals to be $t_{½} \sim 462$ min. In contrast to photolysis in solution, the modified protein in the crystalline state undergoes a large fluorescence increase upon photolysis of caged GTP. A potential explanation for this difference can be deduced from the x-ray structure of p21(mod)·R-caged GTP: The 2-nitrophenylethyl (cage) group of caged GTP and the NBD fluorophore form strong cation-π/π-π stacking interactions with two residues (Arg-102, Tyr-64) from a neighboring molecule (Fig. 5). This sandwich-like structure falls apart upon removal of the cage group after photolysis of caged GTP, reducing the probability for thermal relaxation pathways of the excited fluorophore and therefore increasing the fluorescence quantum yield.

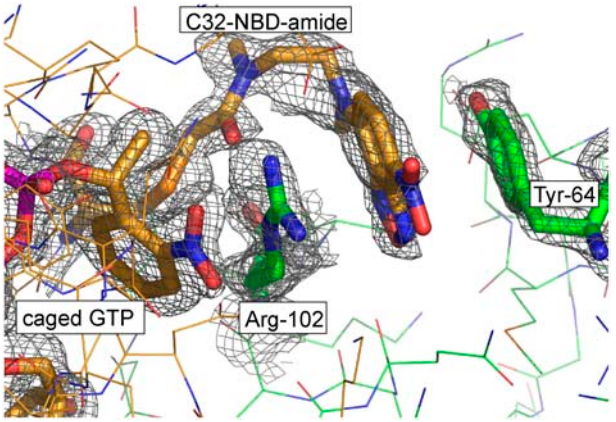

FIGURE 5 Representation of the structural environment for the NBD fluorophore and the 2-nitrophenylethyl (2-NPE, cage) group of caged GTP. The aromatic moieties (*yellow sticks*) form a strong π-stacking interaction with two residues from a neighboring molecule (Arg-102, Tyr-64, *green sticks*). The displayed $2F_{Obs}$-$1F_{Calc}$ electron density map was calculated after refinement of the model structure with the program Refmac 5 (38) (1σ cutoff level, displayed with the program Pymol (39)).To reduce model bias, residues C32-NBD-amide, Tyr-64, Arg-102, and the nucleotide were omitted during the refinement and for map calculation.

The direct measurement of fluorescence changes after caged GTP photolysis can complement information about the extent of photolysis obtained by other methods, such as HPLC analysis of the protein crystal after data collection (25). However, HPLC analysis alone can give misleading results: After collection of a complete data set from crystals of p21(mod)·caged GTP at 100 K on a synchrotron x-ray source, HPLC measurements showed almost complete cleavage of caged GTP. This was even the case if the crystals were never exposed to UV light, indicating that x-ray-induced radiolysis of caged GTP occurred. Interestingly, the x-ray structure of these crystals displayed clear electron density for nonphotolyzed caged GTP (Fig. 5), in contradiction to the HPLC results. We conclude that with the high intensity of modern synchrotron x-ray sources, caged GTP complexed to H-ras p21 can be radiolyzed efficiently even at 100 K. Although the covalent bond between the cage group and the nucleotide is broken, the reaction products cannot diffuse within the crystal due to the low temperature. Therefore, the x-ray structure of the protein resembles the nonphotolyzed form. In this biological model system, fluorescence changes are dependent on conformational changes within the protein and not only on the photochemical cleavage of caged GTP. Whereas with HPLC the photolysis reaction itself is investigated, with fluorescence measurements the conformational changes of the protein in response to photolysis of caged GTP can be analyzed.

To obtain the GTP-bound intermediate state of the protein, several crystals with similar shape and size, grown under identical conditions, were photolyzed at room temperature.

The state of the crystals could be analyzed directly by continuously measuring the fluorescence spectrum (Fig. 6), assuming complete photolysis when no further change of the fluorescence intensity was observed. It could be verified by HPLC analysis on photolyzed and dissolved crystals that the completion of fluorescence changes upon photolysis coincides with the completion of photolysis of all caged GTP molecules in the crystals. However, it should be kept in mind for experiments without the option of such a control experiment that from the fluorescence increase alone it would not be possible to decide if all molecules or only a small fraction of molecules changed their properties upon illumination.

Interestingly, crystals that were photolyzed in a hanging drop setup showed a significantly higher fluorescence increase than crystals that were photolyzed in a cryo-loop, stabilized by a humid nitrogen stream (4.9-, 5.2-, and 5.4-fold fluorescence increase in three analyzed crystals from a hanging drop setup compared to a 2.8- and 3.4-fold fluorescence increase in loop-mounted crystals). The comparison of x-ray diffraction data from both types of crystals revealed differences in the electron density around the γ-phosphate group of the nucleotide: Crystals photolyzed in a cryo-loop displayed significant electron density at the position of the (released) cage group (Fig. 7 *A*), whereas almost no electron density was visible in crystals photolyzed in hanging drops (Fig. 7 *B*).

In contrast to crystals in hanging drops, the loop-mounted crystals had almost no surrounding buffer reservoir. Therefore, the diffusion of the cage group is limited, and it remains in the vicinity of its original position. Additional effects, such as shrinking of the crystal due to low relative humidity values of the humid gas stream, could also strongly affect the diffusion of the cage group. In this respect, fluorescence spectroscopy is an efficient and nondestructive method to obtain information about the state of a macromolecular crystal in kinetic crystallography. To verify that the strong fluorescence increase upon photolysis is caused mainly by conformational changes and not by the photolytical formation of a nitronic acid (34), p21(mod)·R-caged GTP crystals were investigated after short UV exposures at different temperatures (Fig. 8). At room temperature, no further fluorescence increase was observed after turning off the UV light. In contrast, at lower temperatures, a propagation of the fluorescence increase was observed after stopping the UV exposure. The reaction rate on the timescale of seconds at lower temperatures might either be an effect of dark reactions subsequent to photolysis of caged GTP, which result in the release of GTP and the cage group, and/or by conformational rearrangements in the protein environment of the nucleotide.

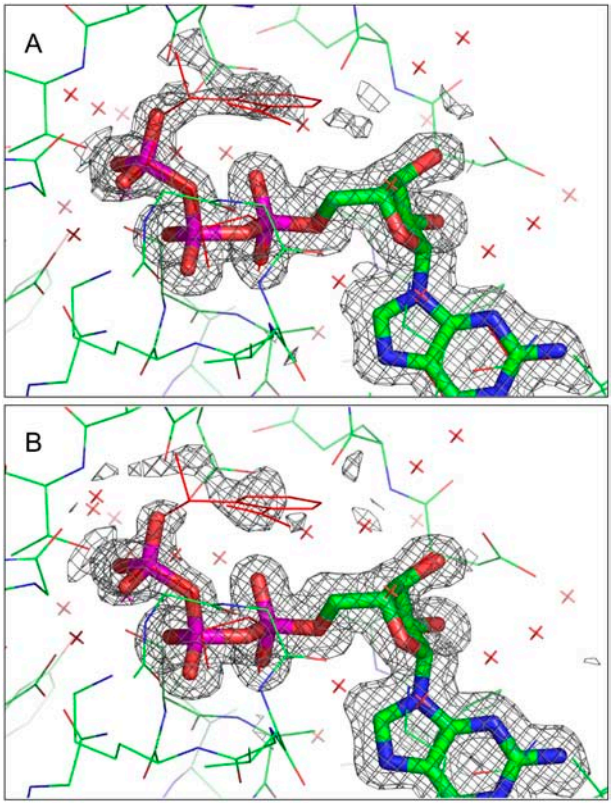

FIGURE 7 Environment of the nucleotide in crystals of p21(mod)·R-caged GTP. (*A*) Display of the structure from a crystal that was photolyzed in a nylon-loop. (*B*) Display of the structure from a crystal photolyzed in a hanging drop setup. For both crystal types, the completeness of caged GTP photolysis was verified by HPLC analysis. The displayed $1F_{Obs}$-$1F_{Calc}$ electron density map was calculated after refinement of the model structure with the program Refmac 5 (38) (2σ cutoff level, displayed with the program Pymol (39)). The nucleotide was omitted during the refinement and for map calculation.

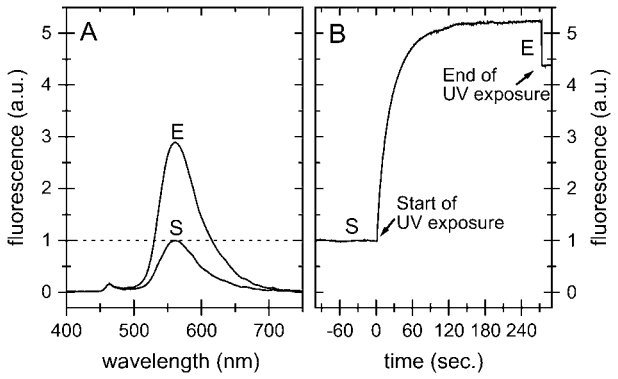

FIGURE 6 Fluorescence spectra of p21(mod)·R-caged GTP. The time point at the start of the photolysis is marked with *S* and the end of photolysis with *E*. (*A*) Fluorescence spectra of a loop-mounted crystal of p21(mod)·R-caged GTP (λ_{Ex} = 441.6 nm) with UV light (325 nm). (*B*) Fluorescence intensity change (λ_{Ex} = 441.6 nm, λ_{Em} = 560 nm) of a crystal of p21(mod)·R-caged GTP upon photolysis in a hanging drop crystal setup. The crystal was photolyzed with UV light (325 nm) until no further changes in fluorescence intensity could be observed. During UV exposure, the fluorescence signal is artificially increased by ~20% due to the additional illumination. It was verified by HPLC that in both setups (Fig. 6, *A* and *B*) complete photolysis of caged GTP was reached, despite the fact that the relative fluorescence increase was different.

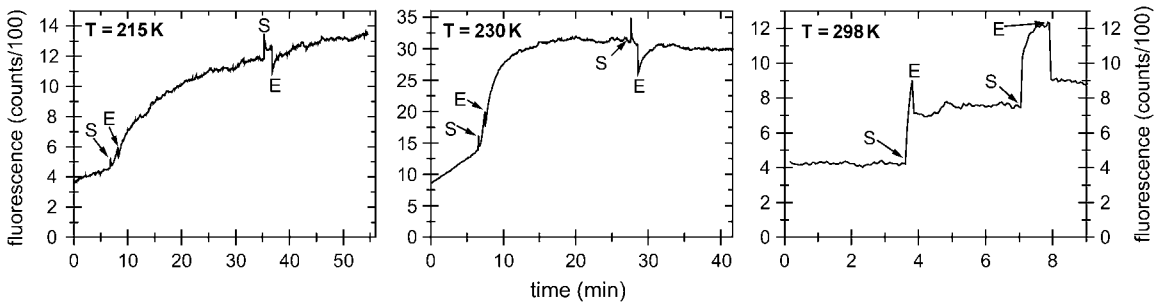

FIGURE 8 Photolysis of crystals of p21(mod)·R-caged GTP at different temperatures. The fluorescence excitation was performed with blue light (λ_{Ex} = 441.6 nm). The start of UV light exposure (325 nm) is marked with *S* and the end of UV exposure with *E*. The baseline drift at 215 K and 230 K is most probably due to a slow degeneration of crystal order, which results in a higher flexibility of the fluorophore and therefore increased fluorescence quantum yield. The loss of crystal order was proved by collecting x-ray diffraction images during the experiment at an x-ray home source (Oxford Diffraction, Xcalibur PX Ultra).

An effect solely due to the photolytical formation of a nitronic acid can be excluded, as this takes place on the submillisecond timescale (34). Interestingly, complete UV photolysis could not be achieved at 100 K even after ~100 min of UV exposure (data not shown). At cryogenic temperatures, x-ray radiolysis of caged compounds could be an alternative method to trigger fast enzymatic reactions (10), as will be discussed in the next section.

Influence of synchrotron x-ray radiation on crystals of the modified H-Ras p21 monitored by fluorescence spectroscopy

Synchrotron x-ray radiation can induce significant changes in protein crystals, for example by reduction of the crystal quality (x-ray damage) (35) or by radiolysis of caged compounds (10,36). Since enzymatic reactions in a protein crystal are prevented at sufficiently low temperatures, using radiolysis of caged compounds was suggested as a reaction trigger for systems that cannot be triggered efficiently at ambient temperatures (10). Since the degree of changes (undesired or desired) cannot be monitored easily during and by the x-ray diffraction experiment, we used the FLUMIX spectrometer to investigate the changes of fluorescence caused by intensive x-ray exposure at ambient and at cryogenic temperatures.

In a first set of experiments, we measured the half-life of x-ray-induced radiolysis of caged GTP in crystals of p21(mod)·R-caged GTP at 302.5 K (Fig. 9). The fluorescence intensity displays a monoexponential increase with a half-time of $t_{½} = 138.5 \pm 2.1$ s x-ray exposure (corrected by the readout time during which the x-ray shutter was closed). UV illumination after the x-ray exposure showed no further increase in fluorescence intensity of the crystals, indicating complete cleavage of caged GTP by the x-ray exposure. As a negative control, the experiment was repeated with crystals of p21(mod)·GppNHp (guanosine-5′-(β,γ-imido)-triphosphate, a nonhydrolysable GTP analog) that do not contain a photolyzable nucleotide analog. As expected, no significant increase in the fluorescence signal at 560 nm was observed upon x-ray exposure of these crystals (Fig. 9). We conclude that the observed monoexponential fluorescence increase in crystals of p21(mod)·R-caged GTP can be attributed to the radiolysis of caged GTP and subsequent conformational rearrangements (see Properties of the modified H-Ras p21 in the crystalline state).

Besides the x-ray-induced radiolysis of caged GTP, we observed additional effects of x-ray illumination: Within the first 10 s of x-ray exposure, a strong fluorescence decrease was observed in p21(mod)·GppNHp crystals at 302.5 K, which is followed by a fast buildup of species with a blue-shifted fluorescence spectrum within ~1 min. The observed fluorescence decrease coincides well with the loss of diffraction power of the p21(mod)·GppNHp crystals within the first seconds of x-ray exposure. The crystals lost essentially all diffraction power within ~20 s of x-ray exposure. We found that the stability to x-ray illumination was different for crystals cocrystallized with different nucleotides: Crystals of p21(mod)·R-caged GTP had a significantly higher initial diffraction power and a slower x-ray-induced diffraction loss (>200 s of x-ray exposure) than crystals of p21(mod)·GppNHp. It is probable that in crystals of p21(mod)·R-caged GTP, the increase in fluorescence intensity upon radiolysis of caged GTP overcompensates the relatively slow decrease in fluorescence due to the loss of crystal order and associated rearrangements within the environment of the fluorophore. This assumption is supported by two observations: First, the total fluorescence increase upon complete x-ray radiolysis of caged GTP in p21(mod)·R-caged GTP crystals was relatively small, which might indicate a low crystal quality of the achieved intermediate state (a factor of ~2.3 in comparison to factors of 2.8–5.4 in UV photolysis experiments, see Properties of the modified H-Ras p21 in the crystalline state). Second, a lag phase of ~20 s between the start of x-ray exposure and the beginning of a fluorescence increase was observed. This lag phase might be explained by the

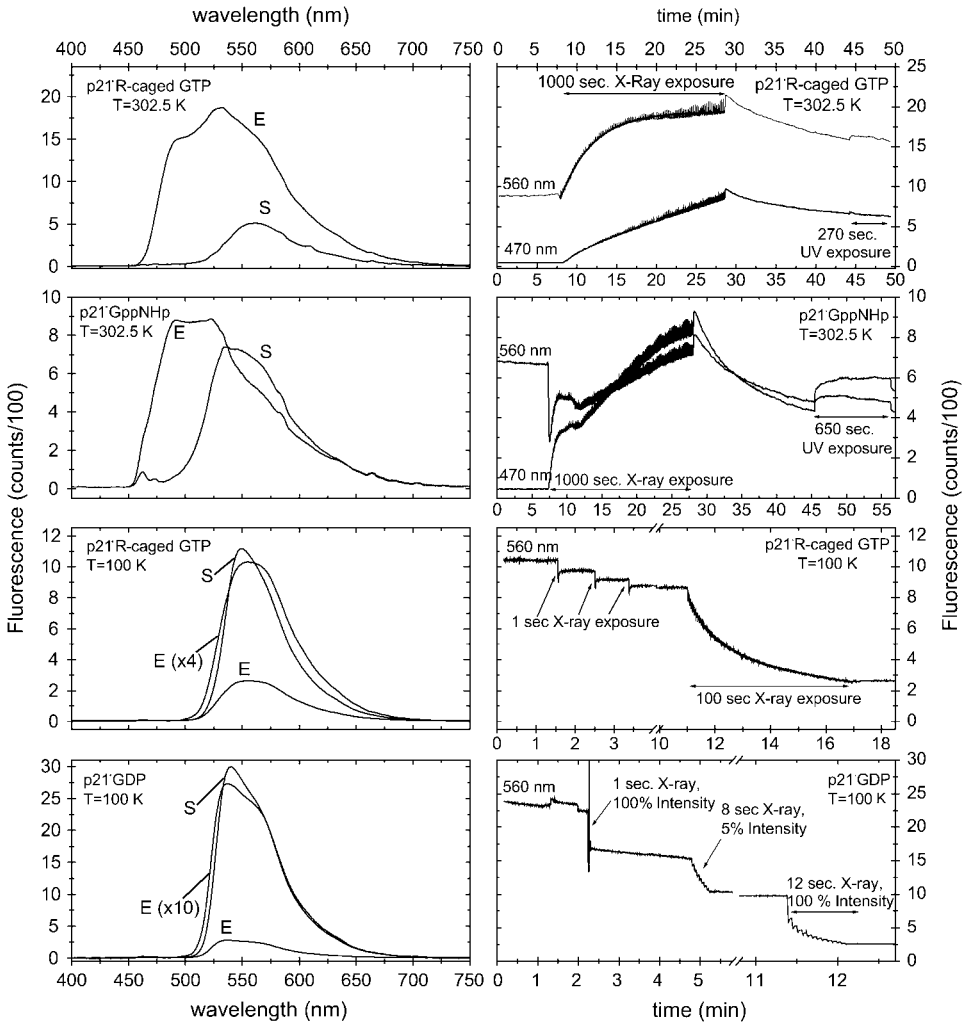

FIGURE 9 Effect of x-ray radiation on crystals of p21(mod). On the left panel, fluorescence emission spectra (λ_{Ex} = 441.6 nm) are shown before (*S*) and after (*E*) x-ray exposure. The corresponding time traces of the fluorescence change at representative emission wavelengths are shown in the right panel. The protein crystals were mounted in 0.05–0.1-mm nylon loops and were stabilized either with a cold nitrogen stream (100 K) or a humid nitrogen stream with 97.5% relative humidity (302.5 K). During x-ray exposure, x-ray diffraction images were constantly measured. Each image started at the same crystal ϕ angle, and a rotation range of 0.1° was used for each image. The x-ray shutter was closed during the image readout time (~2.5 s/image). The total x-ray exposure times are marked in the time traces (100% intensity equals 4×10^{10} phts/s). After x-ray exposure at 302.5 K, the crystals were illuminated with UV light (λ_{Ex} = 325 nm) with an intensity of ~0.1 mW.

competing effects of a decrease in fluorescence caused by x-ray-induced diffraction loss of the crystals, with a fluorescence increase due to radiolysis of caged GTP. In addition, the formation of species with a blue-shifted fluorescence emission maximum upon x-ray exposure was also observed in crystals of p21(mod)·R-caged GTP. However, the formation of these species was significantly slower than in p21(mod)·GppNHp, consistent with the higher stability to x-ray radiation of these crystals. After closing the x-ray shutter, the fluorescence signal at 470 and 560 nm decays both in crystals of p21(mod)·GppNHp and p21(mod)·caged GTP. This decay could be explained by the formation of reactive species (e.g., radicals) and/or bond rearrangements within the fluorophore environment, which can continue to disrupt the protein crystal after closing the x-ray shutter either directly or by increasing the vulnerability of the fluorophore for photobleaching by the ongoing UV exposure.

In a second set of experiments, we performed optical fluorescence studies during x-ray diffraction experiments at cryogenic temperatures. Due to x-ray exposure, crystals of p21(mod)·R-caged GTP displayed a fast decay of optical fluorescence that was already significant after 1 s of x-ray exposure (Fig. 9). It is unlikely that the observed fluorescence change is solely due to the radiolysis of caged GTP, since the fluorescence change is negative and on a faster timescale than the fluorescence change observed for p21(mod)·R-caged GTP crystals at room temperature (Fig. 9). Furthermore, an even more pronounced fluorescence decay was observed if the experiment was repeated with crystals of p21(mod)·GDP that do not contain a photolabile nucleotide. With these crystals, a single 1 s x-ray exposure reduced the fluorescence intensity by 25%, and eight additional pulses with the x-ray beam attenuated to ~5% of the maximal intensity (~2×10^9 phts/s, 1 s/puls) gave another 32% decay in fluorescence intensity. These results are quite unexpected, since the fluorescence changes occur with x-ray doses that are small in comparison to normal exposures needed for the collection of a complete x-ray diffraction data set. It is important to note that for both crystal types (p21(mod)·caged GTP and p21(mod)·GDP), the fluorescence changes upon x-ray exposure at 100 K were not correlated with an obvious loss of diffraction power of the crystals.

SUMMARY AND CONCLUSIONS

We have presented a new fluorescence microspectrophotometer for use in kinetic crystallography in combination with x-ray diffraction experiments. The FLUMIX setup with a 0° design can be used in combination with x-ray diffraction on many synchrotron beamlines without the need of a specialized mechanical support. Due to the optimized setup, the FLUMIX device is very versatile and can also be used for other applications, for example, for fluorescence measurements or reaction initiation directly in hanging drops.

As a biological model system, a modified form of H-Ras p21 was used. A photo-excitable GTP precursor (caged GTP) and an artificial fluorophore were introduced into this slow GTPase to show the wide applicability of fluorescence measurements even on protein crystals without an intrinsic reaction trigger or fluorophore. We found that in addition to a relatively small change in fluorescence upon GTP hydrolysis, the accumulation of the GTP-bound intermediate state after photolysis involves a large fluorescence increase due to conformational rearrangements within the protein. The relative fluorescence increase depends not only on the completeness of caged GTP photolysis but also on the quality of the accumulated intermediate. Limited diffusion of the cage group due to a low amount of reservoir solution surrounding the crystal or loss of crystal order can lead to a lower relative increase, which is an indication of poor crystal quality of the formed intermediate state. In this respect, fluorescence measurements can be used to optimize the accumulation of the GTP-bound intermediate state of H-Ras p21.

X-ray radiolysis experiments on a synchrotron beamline at 100 K showed a fast fluorescence decay that takes place within a few seconds of x-ray exposure in some cases. This fluorescence decay is not connected with an obvious loss of diffraction power of the crystals. The timescale for fluorescence decay is small in comparison to a typical exposure time needed for the collection of a complete x-ray diffraction data set. According to these results, x-ray radiolysis of caged compounds at cryogenic temperatures might involve several problems. Conditions for triggering a reaction have to be optimized to radiolyze the caged compounds without further undesired x-ray-induced changes within the protein crystal. In this respect, optical fluorescence measurements have proven to be useful as a highly sensitive method to monitor small changes in a protein crystal that cannot easily be seen as a change in the diffraction quality of the crystal. Fluorescence measurements can be very helpful for the selection of optimal radiolysis conditions such as intensity, x-ray wavelength, temperature, and x-ray exposure time. Since large fluorescence changes are observable even upon relatively mild x-ray exposures and even in systems without a photolabile nucleotide, the application of optical fluorescence measurements in correlation with x-ray diffraction seems to be a very promising tool to quantify the degree of x-ray-induced changes (i.e., radiation damage) during the collection of x-ray diffraction data.

In general, the FLUMIX device offers a unique, nondestructive method to obtain detailed information about the state of a protein crystal. The system was mainly developed for use in x-ray crystallography but can also be used in many other areas where fluorescence measurements in nanovolumes are desired.

We are grateful to Sascha Gentz for providing us with purified GDP and GppNHp, John E. T. Corrie for providing us with isomeric pure caged GTP, and Astrid U. Krämer for the Y32C,C118S mutant of H-Ras p21. We thank Ilme Schlichting for sharing equipment, Georg Holtermann and Igor Chizhov for technical support and fruitful discussions, and Tammy Woo for helpful comments on the manuscript. Additionally, we thank the beamline staff of ID14 and ID29 at ESRF (Grenoble, France) and PXI (PSI Villigen, Switzerland) for technical support. Coordinates for the structures of p21(mod) which are discussed in this work will be deposited in the Protein Data Bank (37) (PDB entry codes 2CL10, 2CE2, 2CL6, 2EVW, 2CL7, 2CLD, 2CLC).

This research was funded by the Bundesministerium für Bildung und Forschung (grant 05 KS1EDA/3).

REFERENCES

1. Hajdu, J., R. Neutze, T. Sjogren, K. Edman, A. Szoke, R. C. Wilmouth, and C. M. Wilmot. 2000. Analyzing protein functions in four dimensions. *Nat. Struct. Biol.* 7:1006–1012.
2. Mozzarelli, A., and G. L. Rossi. 1996. Protein function in the crystal. *Annu. Rev. Biophys. Biomol. Struct.* 25:343–365.
3. Ren, Z., B. Perman, V. Srajer, T. Y. Teng, C. Pradervand, D. Bourgeois, F. Schotte, T. Ursby, R. Kort, M. Wulff, and K. Moffat. 2001. A molecular movie at 1.8 A resolution displays the photocycle of photoactive yellow protein, a eubacterial blue-light receptor, from nanoseconds to seconds. *Biochemistry.* 40:13788–13801.
4. Scheidig, A. J., C. Burmester, and R. S. Goody. 1999. The prehydrolysis state of p21(ras) in complex with GTP: new insights into the role of water molecules in the GTP hydrolysis reaction of ras-like proteins. *Struct. Fold. Des.* 7:1311–1324.
5. Schlichting, I. 2000. Crystallographic structure determination of unstable species. *Acc. Chem. Res.* 33:532–538.
6. Stoddard, B. L. 1998. New results using Laue diffraction and time-resolved crystallography. *Curr. Opin. Struct. Biol.* 8:612–618.
7. Sjogren, T., G. Carlsson, G. Larsson, A. Hajdu, C. Andersson, H. Pettersson, and J. Hajdu. 2002. Protein crystallography in a vapour stream: data collection, reaction initiation and intermediate trapping in naked hydrated protein crystals. *J. Appl. Cryst.* 35:113–116.
8. Kiefersauer, R., M. E. Than, H. Dobbek, L. Gremer, M. Melero, S. Strobl, J. M. Dias, T. Soulimane, and R. Huber. 2000. A novel free-mounting system for protein crystals: transformation and improvement of diffraction power by accurately controlled humidity changes. *J. Appl. Cryst.* 33:1223–1230.
9. Stoddard, B. L., and G. K. Farber. 1995. Direct measurement of reactivity in the protein crystal by steady-state kinetic studies. *Structure.* 3:991–996.
10. Ursby, T., M. Weik, E. Fioravanti, M. Delarue, M. Goeldner, and D. Bourgeois. 2002. Cryophotolysis of caged compounds: a technique for trapping intermediate states in protein crystals. *Acta Crystallogr. D Biol. Crystallogr.* 58:607–614.
11. Specht, A., T. Ursby, M. Weik, L. Peng, J. Kroon, D. Bourgeois, and M. Goeldner. 2001. Cryophotolysis of ortho-nitrobenzyl derivatives of enzyme ligands for the potential kinetic crystallography of macromolecules. *ChemBioChem.* 2:845–848.
12. Scheidig, A. J., C. Burmester, and R. S. Goody. 1998. Use of caged nucleotides to characterize unstable intermediates by x-ray crystallography. *Methods Enzymol.* 291:251–264.

13. O'Hara, P., P. Goodwin, and B. L. Stoddard. 1995. Direct measurement of diffusion rates in enzyme crystals by video absorbance spectroscopy. *J. Appl. Cryst.* 28:829–834.

14. Stoddard, B. L. 2001. Trapping reaction intermediates in macromolecular crystals for structural analyses. *Methods.* 24:125–138.

15. Berglund, G. I., G. H. Carlsson, A. T. Smith, H. Szoke, A. Henriksen, and J. Hajdu. 2002. The catalytic pathway of horseradish peroxidase at high resolution. *Nature.* 417:463–468.

16. Schlichting, I., S. C. Almo, G. Rapp, K. Wilson, K. Petratos, A. Lentfer, A. Wittinghofer, W. Kabsch, E. F. Pai, G. A. Petsko, and R. S. Goody. 1990. Time-resolved x-ray crystallographic study of the conformational change in Ha-Ras p21 protein on GTP hydrolysis. *Nature.* 345:309–315.

17. Duke, E. M., S. Wakatsuki, A. Hadfield, and L. N. Johnson. 1994. Laue and monochromatic diffraction studies on catalysis in phosphorylase b crystals. *Protein Sci.* 3:1178–1196.

18. Goody, R. S., E. F. Pai, I. Schlichting, H. Rensland, A. Scheidig, S. Franken, and A. Wittinghofer. 1992. Studies on the structure and mechanism of H-ras p21. *Philos. Trans. R. Soc. Lond. B Biol. Sci.* 336: 3–10.

19. Hadfield, A., and J. Hajdu. 1993. A fast and portable microspectrophotometer for protein crystallography. *J. Appl. Cryst.* 26: 839–842.

20. Chen, Y., V. Srajer, K. Ng, A. LeGrand, and K. Moffat. 1994. Optical monitoring of protein crystals in time-resolved x-ray experiments: microspectrophotometer design and performance. *Rev. Sci. Instrum.* 65:1506–1511.

21. Bourgeois, D., X. Vernede, V. Adam, E. Fioravanti, and T. Ursby. 2002. A microspectrophotometer for UV-visible absorption and fluorescence studies of protein crystals. *J. Appl. Cryst.* 35:319–326.

22. Sakai, K., Y. Matsui, T. Kouyama, Y. Shiro, and S. I. Adachi. 2002. Optical monitoring of freeze-trapped reaction intermediates in protein crystals: a microspectrophotometer for cryogenic protein crystallography. *J. Appl. Cryst.* 35:270–273.

23. Weik, M., X. Vernede, A. Royant, and D. Bourgeois. 2004. Temperature derivative fluorescence spectroscopy as a tool to study dynamical changes in protein crystals. *Biophys. J.* 86:3176–3185.

24. Karlsson, A., J. V. Parales, R. E. Parales, D. T. Gibson, H. Eklund, and S. Ramaswamy. 2000. The reduction of the Rieske iron-sulfur cluster in naphthalene dioxygenase by x-rays. *J. Inorg. Biochem.* 78:83–87.

25. Schlichting, I., G. Rapp, J. John, A. Wittinghofer, E. F. Pai, and R. S. Goody. 1989. Biochemical and crystallographic characterization of a complex of c-Ha-ras p21 and caged GTP with flash photolysis. *Proc. Natl. Acad. Sci. USA.* 86:7687–7690.

26. Stouten, P. F., C. Sander, A. Wittinghofer, and A. Valencia. 1993. How does the switch II region of G-domains work? *FEBS Lett.* 320:1–6.

27. Haugland, R. P. 2002. Handbook of Fluorescent Probes and Research Products. I. Molecular Probes, editor. Molecular Probes, Eugene, OR.

28. Scheidig, A. J., A. Sanchez-Llorente, A. Lautwein, E. F. Pai, J. E. Corrie, G. P. Reid, A. Wittinghofer, and R. S. Goody. 1994. Crystallographic studies on p21(H-ras) using the synchrotron Laue method: improvement of crystal quality and monitoring of the GTPase reaction at different time points. *Acta Crystallogr. D Biol. Crystallogr.* 50:512–520.

29. Eisinger, J., and J. Flores. 1979. Front-face fluorometry of liquid samples. *Anal. Biochem.* 94:15–21.

30. McPherson, A. 2004. Introduction to protein crystallization. *Methods.* 34:254–265.

31. Scheidig, A. J., S. M. Franken, J. E. Corrie, G. P. Reid, A. Wittinghofer, E. F. Pai, and R. S. Goody. 1995. X-ray crystal structure analysis of the catalytic domain of the oncogene product p21H-ras complexed with caged GTP and mant dGppNHp. *J. Mol. Biol.* 253:132–150.

32. Scherer, A., J. John, R. Linke, R. S. Goody, A. Wittinghofer, E. F. Pai, and K. C. Homes. 1989. Crystallization and preliminary x-ray analysis of the human c-H-ras-oncogene product p21 complexed with GTP analogues. *J. Mol. Biol.* 206:257–259.

33. John, J., I. Schlichting, E. Schiltz, P. Rosch, and A. Wittinghofer. 1989. C-terminal truncation of p21H preserves crucial kinetic and structural properties. *J. Biol. Chem.* 264:13086–13092.

34. Corrie, J. E., A. Barth, V. R. Munasinghe, D. R. Trentham, and M. C. Hutter. 2003. Photolytic cleavage of 1-(2-nitrophenyl)ethyl ethers involves two parallel pathways and product release is rate-limited by decomposition of a common hemiacetal intermediate. *J. Am. Chem. Soc.* 125:8546–8554.

35. Nave, C., and E. F. Garman. 2005. Towards an understanding of radiation damage in cryocooled macromolecular crystals. *J. Synchrotron Radiat.* 12:257–260.

36. Schlichting, I., and R. S. Goody. 1997. Triggering methods in crystallographic enzyme kinetics. *In* Methods in Enzymology, Vol. 277. C. Carter, R. M. Sweet, editors. Academic Press, San Diego, CA. 467–490.

37. Berman, H. M., J. Westbrook, Z. Feng, G. Gilliland, T. N. Bhat, H. Weissig, I. N. Shindyalov, and P. E. Bourne. 2000. The protein data bank. *Nucleic Acids Res.* 28:235–242.

38. Collaborative Computational Project, Number 4. 1994. The CCP4 suite: programs for protein crystallography. *Acta Crystallogr. D Biol. Crystallogr.* 50:760–763.

39. Delano, W. L. 2002. The pymol molecular graphics system. http://www.pymol.org.